Surface Science 604 (2010) 1481–1486

Contents lists available at ScienceDirect

Surface Science

journal homepage: www.elsevier.com/ locate/susc

Thermodynamic driving forces governing assembly of disilicide nanowires

Aniketa Shinde [a,b], Ruqian Wu [a], Regina Ragan [b,*]

[a] Department of Physics and Astronomy, 4129 Frederick Reines Hall, University of California Irvine, Irvine, CA 92697-4575, USA
[b] Department of Chemical Engineering and Materials Science, 916 Engineering Tower, University of California Irvine, Irvine, CA 92697-2575, USA

ARTICLE INFO

Article history:
Received 20 November 2009
Accepted 10 May 2010
Available online 20 May 2010

Keywords:
Scanning probe microscopy
Ab initio calculations
Rare earth disilicide
Metal nanowires
Self assembly

ABSTRACT

Driving forces are investigated for assembling low dimensional, metallic, erbium and dysprosium disilicide nanowires on Si(001), using both scanning probe microscopy and density functional theory. Side-by-side comparison between emulated and measured scanning tunneling microscopy images allows establishment of reliable atomic models for complex adatom surface reconstructions of Er/Si(001) and Dy/Si(001) that are precursors to high aspect ratio disilicide nanowires. Peculiar surface reconstructions and relaxation of Si bonds are identified as the key factors for nucleation of these disilicide nanowires in parallel arrays on vicinal Si(001). Stable nanowire widths and heights are calculated with predicted atomic models that are consistent with experimental observations. A clear understanding of the nanowire–substrate interface is determined by correlating adatom reconstruction patterns with nanowire formation that is imperative to the development of unique procedures for massive fabrication of monodisperse nanosystems.

1. Introduction

Metal nanostructures exhibit unique physical properties and are promising for broad applications including catalysis, sensors, nanoelectronics, optical communication and quantum computing. Self-assembled structures such as carbon nanotubes [1] and yttrium disilicide nanowires [2,3] permit observation of one-dimensional transport in metallic systems, which are important for the advancement of both fundamental science and innovative nanotechnology. Lithographic means typically cannot fabricate metal nanostructures at length scales where quantum size effects are observed. It is therefore crucial to study the atomic interactions that govern self assembly of functional nanosystems with different building blocks. Atomic interactions not only yield interesting physical phenomena, these mechanisms are also critical for the control of growth patterns. Rare earth disilicide nanowires ($RESi_{2-x}$) are of considerable interest since they self-assemble on Si(001) [4–7] and have high conductivity [8–11] and low Schottky barrier height on *n*-type silicon [12], with strong potential for integration with present Si technologies. Disilicide nanostructures fabricated in ultra high vacuum (UHV) can be probed *in situ* so it is possible to correlate morphology and electronic properties and to further examine quantum confinement effects in low dimensional metallic systems. Furthermore, uniform high-density $RESi_{2-x}$ nanowires (RE = Er, Dy) can be used as templates for Au [13] or Pt [14] clusters which have been demonstrated to be important nanocatalysts [15,16]. Overall, $RESi_{2-x}$ nanostructures represent a multi-purpose low dimensional system and it is indispensable to understand the physical processes governing their assembly, starting from the adsorption of metal adatoms. Although the driving force for disilicide nanowire formation on Si(001) has been attributed to the asymmetric strain between $RESi_{2-x}$ in the hexagonal aluminum diboride (AlB_2) type lattice and the Si(001) diamond cubic lattice [10,17], forces leading to nanowire nucleation with particular size and orientation have not been satisfactorily elucidated.

Using density functional theory (DFT) calculations and scanning tunneling microscopy (STM) analysis, our previous investigations predicted stable arrangements of Y adatoms in the wetting layer on Si (001) [19–21] at various adatom coverages and explained adatom geometries in experimentally observed RE/Si(001) surface reconstructions such as (2×3), [6,22,23] (2×4), [19,24–27] and (2×7) [24,26–28] reported in the literature. The predicted surface dipole established by charge transfer from Y adatoms to Si, confirmed through scanning Kelvin probe force microscopy measurements of RE/Si(001) [20], was found to be crucial for understanding the formation of peculiar reconstruction patterns. In this paper, we provide a platform to answer challenging issues regarding nucleation, nanowire–substrate interface, and morphology of $RESi_{2-x}$ (RE = Er and Dy) nanowires on Si(001). $RESi_{2-x}$ nanowires (RE = Er, Dy, Gd, Sm, Ho) [5,6,26] are reported to orient with the long axis perpendicular to Si dimer rows on (2×1) reconstructed vicinal Si (001) surfaces; however the atomistic interactions driving this phenomenon and nanowire–substrate interface have not been explained. Synergistic STM characterization of Er/Si(001) and Dy/Si

* Corresponding author.
E-mail address: rragan@uci.edu (R. Ragan).

0039-6028/$ – see front matter © 2010 Elsevier B.V. All rights reserved.
doi:10.1016/j.susc.2010.05.012

(001) and *ab initio* calculations of Y/Si(001) reveal stable adsorption geometries of the wetting layer that lead to nanowire orientation perpendicular to Si dimer rows and thereby in unidirectional nanowire arrays on vicinal Si(001) surfaces. Formation energy calculations for narrow YSi_2 nanowires provide insight into the mechanisms that stabilize YSi_2 nanowire structures, such as internal strain relaxation and nanowire surface reconstruction that are found to be relevant to $RESi_{2-x}$ nanowires.

2. Materials and methods

Experimentally, Si(001) (2×1) reconstructed surfaces were prepared and rare earth deposition was performed in ultra high vacuum using methods published in our previous work [19]. Dysprosium or erbium was evaporated from a molybdenum crucible in an electron beam evaporator onto *p*-type Si(001) substrates with dopant density of approximately 10^{18} cm^{-3} at a substrate temperature of 600 °C and annealed post growth for 2 min. Samples were transferred to the analysis chamber without exposure to ambient conditions. Scanning tunneling microscopy imaging was performed at room temperature in UHV and parameters have been published previously as well [19–21].

First principles calculations were performed within the density functional framework using the generalized gradient approximation (GGA) for the description of exchange-correlation effect, as implemented in the Vienna *ab initio* Simulation package (VASP) [29]. To circumvent the difficulty in dealing with the strongly localized 4*f* shell of RE atoms, we used yttrium to represent RE elements, as was demonstrated to be a good substitute in our previous work [19–21]. Y is a trivalent atom that does not have *f* valence electrons but has chemical and physical properties very similar to the RE elements [30]. For example, the atomic and electronic structures of YSi_2 monolayers on Si(111) were found to resemble $RESi_{2-x}$ thin films using low energy electron diffraction and density functional calculations [31,32]. Furthermore, the lattice parameters of hexagonal YSi_2 ($a=0.384$, $c=0.414$ nm, and $c/a=1.08$) are close to those of $RESi_{2-x}$ experimentally characterized in this work (e.g., $a=0.383$ nm, $c=0.412$ nm, and $c/a=1.08$, for $DySi_{2-x}$; and $a=0.379$ nm, $c=0.409$ nm, and $c/a=1.08$, for $ErSi_{2-x}$) [33]. Ultra-soft pseudopotentials (US PP) were used to represent the electron interaction with ionic cores [34]. The plane-wave basis set was constructed with an energy cutoff of 300 eV. To explore reconstruction orientation preferences, a (2×6) Si(001) surface, 8 layer cell was used with 6×2×1 *k*-points. YSi_2 nanowires were modeled on (1×10), 6 layer Si(001) cells with 12×1×1 *k*-points, using the experimental lattice parameter of 0.384 nm [35]. The bottom 3 layers of Si were fixed at their bulk positions and dangling bonds were passivated with hydrogen atoms for all cases. All other atoms were allowed to relax, with a criterion that forces are lower than 0.01 eV/Å, along with a vacuum 15 Å thick. Convergence tests were completed to optimize *k*-points.

3. Results and discussion

$RESi_{2-x}$ nanowires self-assemble with the long axis perpendicular to Si dimer rows with respect to the clean Si(001) substrate as is evident on vicinal surfaces [5,6]. Fig. 1(a) shows an STM image of three $ErSi_{2-x}$ nanowires, labeled I, II, and III, having widths of approximately 1 nm, 1 nm and 3 nm, respectively, grown on a vicinal Si(001) substrate with a miscut of 2.5° toward [110]. The inset shows the vicinal Si(001) surface before Er deposition with the same scan angle; the clean Si(001) surface is predominantly covered with Si dimer rows oriented perpendicular to step edges and with double atomic step heights. The dashed white lines highlight dimer rows on A-type terraces, dimer rows oriented parallel to step edges, and the solid white lines highlight dimer rows on B-type terraces, dimer rows oriented perpendicular to step edges. The reason the surface in the inset is predominantly covered with B-type terraces is that the surface energy of B-type terraces with double atomic step height between adjacent terraces is lower than that of A-type terraces with double atomic step height and that of alternating A- and B-type terraces with single atomic step height on vicinal Si (001) with a miscut toward [110] [36]. It is clear from Fig. 1(a) and the inset that nanowires grow with the long axis perpendicular to Si dimer rows on the original clean Si(001) surface. Fig. 1(a) also shows that disilicide formation consumes Si surface atoms and exposes underlying Si terraces since dimer rows are observed parallel to nanowire long axis and step edges after disilicide growth. However, before Er deposition, Si dimer rows are perpendicular to step edges. This rearrangement of surface Si atoms has made it difficult to determine the atomic relationship at the nanowire–substrate interface and how this is related to dimer row reconstruction on clean Si(001). For example, from Fig. 1(a) it may appear that nanowires nucleate at step edges due to a narrow average terrace width, yet on nominally flat surfaces, it is clear that nanowires do not nucleate specifically on step edges [7,37], but can nucleate in the middle of a terrace.

In order to elucidate the nanowire–substrate interface, we examined preferred adatom surface reconstruction patterns in the wetting layer and orientation of adatom chains relative to the clean Si (001) surface dimers. We then compare disilicide nanowire orientation with adatom chain orientation. Binding energies (BE) for Y adatom arrangements in energetically preferred (2×3) and (2×4) reconstruction patterns were calculated and compared for the formation of atomic chains parallel and perpendicular to Si dimer rows (designated to be along [110]), where:

$$BE = \left(E_{Y/Si(001)} - E_{Sisub} - E_Y\right) / N. \quad (1)$$

$E_{Y/Si(001)}$ is the total energy for the relaxed Y/Si(001) system, $E_{Si\ sub}$ is the total energy for the Si(001) 8 layer substrate, E_Y is the total energy for a single Y atom in bulk and N is the number of Y adatoms in the Y/Si(001) system. Fig. 1(d) shows calculated BE per adatom for groups of adatoms on (2×6) supercells with atomic chains aligned perpendicular, shown in Fig. 1(b), and parallel, shown in Fig. 1(c), to Si[110], dimer row direction. Adatom sites are labeled (1,2) for atomic chains having a width of 2 and (1,2,3) for groups having a width of 3 adatoms that were found in our previous work to represent (2×3) and (2×4) reconstruction patterns, respectively [21]. Configuration (b), with the atomic chain along [1$\bar{1}$0], perpendicular to Si dimer rows on the original Si(001) surface (highlighted in gray), is preferred by approximately 100 meV/adatom according to our calculations. Note that thermal energy during the deposition process is 75 meV. Thus, Y adatoms are predicted to prefer to form atomic chains having width of 2 or 3 adatoms perpendicular to dimer rows on (2×1) reconstructed Si (001), which is consistent with experimental observations for Er, [21,23] Dy [19,25], Sm, [6,21] Gd, [24] and Ho [26,27].

We next examine the geometric relationship between the preferred Y adatom arrangements in the wetting layer and the formation of disilicide nanowires having the hexagonal AlB_2 crystal structure [18,38]. As mentioned prior, due to the reorganization of surface Si atoms during disilicide formation [17,40,41] the nucleation site cannot be unambiguously assigned to the step edge nor can the relationship with the clean Si(001) substrate be determined from STM images alone. When one examines the Y adatom arrangements in the energetically preferred four-fold hollow site on Si(001) shown in the adatom reconstruction patterns of Fig. 1(b), [19,39] YSi_2 [1$\bar{1}$20] must be parallel to Si[110], i.e., nanowire long axis is parallel to Si dimer rows in order for a hexagonal YSi_2 cell to have a coherent interface with a Si(001) surface. This orientation is in agreement with atom arrangement in the hexagonal lattice observed in transmission

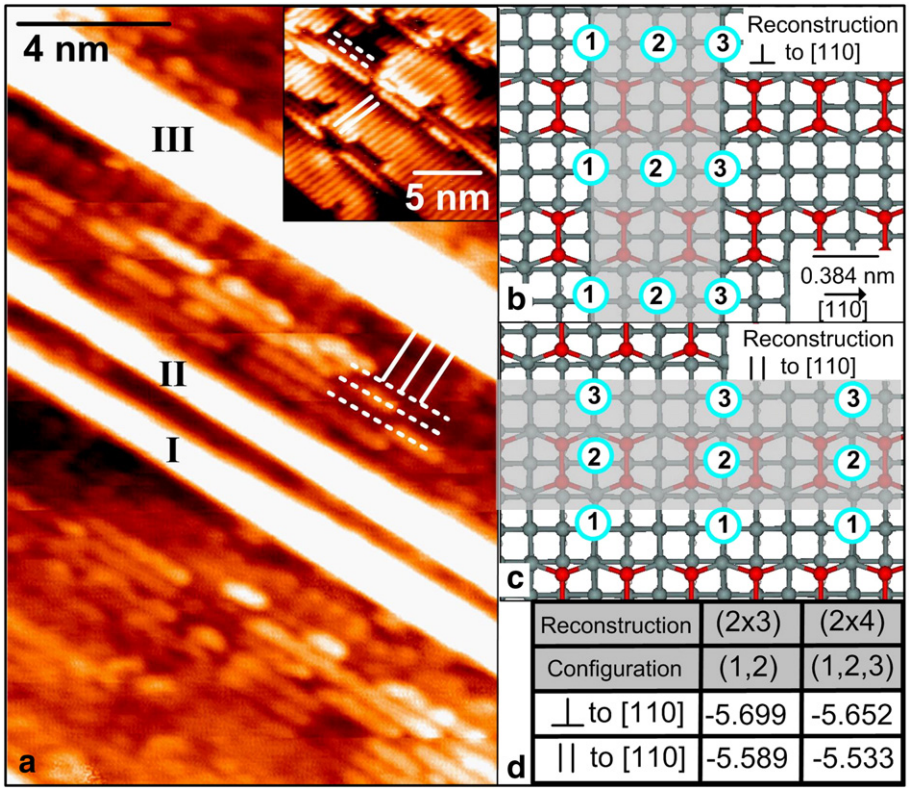

Fig. 1. (a) STM image of three $ErSi_{2-x}$ nanowires (labeled I, II, and III) on miscut Si(001), taken with $V_{bias} = -1.93$ V and 100 pA tunneling current. 20×20 nm inset shows clean miscut Si(001) before Er deposition where dimer row direction on A-type terraces is highlighted by white dashed lines and dimer row direction on B-type terraces is highlighted by solid white lines, taken with $V_{bias} = -2.27$ V. On the right side, ball and stick models for Y adatoms (cyan circles labeled 1, 2, and 3) on four-fold hollow sites on Si(001) with adatom chains (b) perpendicular and (c) parallel to Si[110], dimer row direction. Surface Si dimers are represented by red spheres, bulk Si is represented by dark gray solid spheres, and gray shading highlights the direction of the long axis of adatom chains. (d) Table with binding energy per adatom [eV/Y] for configurations of two adatoms in a row (1,2) and three adatoms in a row (1,2,3) for adatom chains parallel (bottom row) and perpendicular (top row) to Si[110].

electron microscopy images of the cross section along [1120] [38]. Fig. 2(a) is an STM image of one $DySi_{2-x}$ nanowire on flat Si(001) which shows adjacent terraces consisting of both dimer rows perpendicular (terrace B) and parallel (terrace A) to nanowire long axis. What is significant about Fig. 2(a) is that the line profile provided as an inset reveals that the nanowire–substrate interface is on the same plane as surface Si atoms on terrace A. The dimer rows on terrace A are parallel to nanowire length, a necessary condition for a coherent nanowire–substrate interface as discussed above. An atomic schematic is provided in Fig. 2(b) to elucidate the structure: Si dimer rows (red spheres) on terrace A are parallel to YSi_2 [1120] and lie in the same plane as the nanowire–substrate interface; Si dimer rows on terrace B are one atomic layer higher than the nanowire–substrate interface and are perpendicular to YSi_2 [1120].

BE calculations and experimental STM images show that adatoms in the wetting layer form adatom chains perpendicular to Si dimer rows. STM images of $DySi_{2-x}$ nanowires show that nanowires are oriented parallel to Si dimer rows in the plane of the nanowire–substrate interface. These two results indicate that the adatom chain orientation in the wetting layer defines disilicide nanowire orientation on Si(001) since nanowires are observed to orient perpendicular to dimers with respect to the clean Si(001) surface. These results also indicate that surface Si atoms neighboring adatom chains in the wetting layer reorganize and some atoms are consumed for incorporation into disilicide nanowires and thereby reveal dimer rows parallel to the nanowire long axis after nanowire formation. This is in agreement with previous reports observing that the silicon surface reorganizes after nucleation of $RESi_{2-x}$ nanostructures [7,37,41].

Stable nanowire morphologies were investigated by calculating formation energy as a function of nanowire width. Formation energies were calculated for nine nanowires on Si(001) having widths ranging from 1 to 9 a_{Si}. Fig. 3 plots formation energies (FE) of the nanowires versus the inverse of nanowire width, defined as:

$$FE = \left(E_{YSi_2/Si} - E_{Sisub} - N_{YSi_2}E_{YSi_2} - N_{Si}E_{Si}\right) / N_{YSi_2}. \quad (2)$$

$E_{YSi2/Si}$ is the total energy of the system that is composed of the nanowire and Si(001) substrate, E_{Sisub} is the total energy of the Si (001) dimer reconstructed substrate, E_{YSi_2} is the energy of $aYSi_2$ unit cell in bulk, N_{Si} is the number of Si atoms needed to complete the edge of the nanowire, E_{Si} is the energy of a Si atom in bulk, and N_{YSi_2} is the number of YSi_2 cells in the nanowire. The FE compares the energy between a freestanding YSi_2 cell and a YSi_2 cell formed on a Si(001) substrate. The graph of Fig. 3 shows that single layer YSi_2 nanowires with widths less than 3 a_{Si} have relatively high and positive formation energy; they are predicted to be energetically unfavorable in comparison to Y adatom induced surface reconstruction, such as (2×3) and (2×4), indicated by the dashed area on the graph. The FE approaches zero for $N = 3$. In fact, a 3 a_{Si} wide YSi_2 nanowire (~1 nm wide) is consistent with the smallest nanowire width observed in the experiment. Experimental statistics found for single layer $DySi_{2-x}$, $ErSi_{2-x}$ and YSi_{2-x} nanowires have widths ranging between 1 and 10 nm [5,7,37,42]. Examination of the plot of FE in Fig. 3 also shows that the FE increases again for $N = 4$. An alternating high–low trend in energies is found for calculated FE; FE = 0.10 eV, 0.26 eV, −0.005 eV, 0.01 eV and −0.071 for $N = 3$, 4,

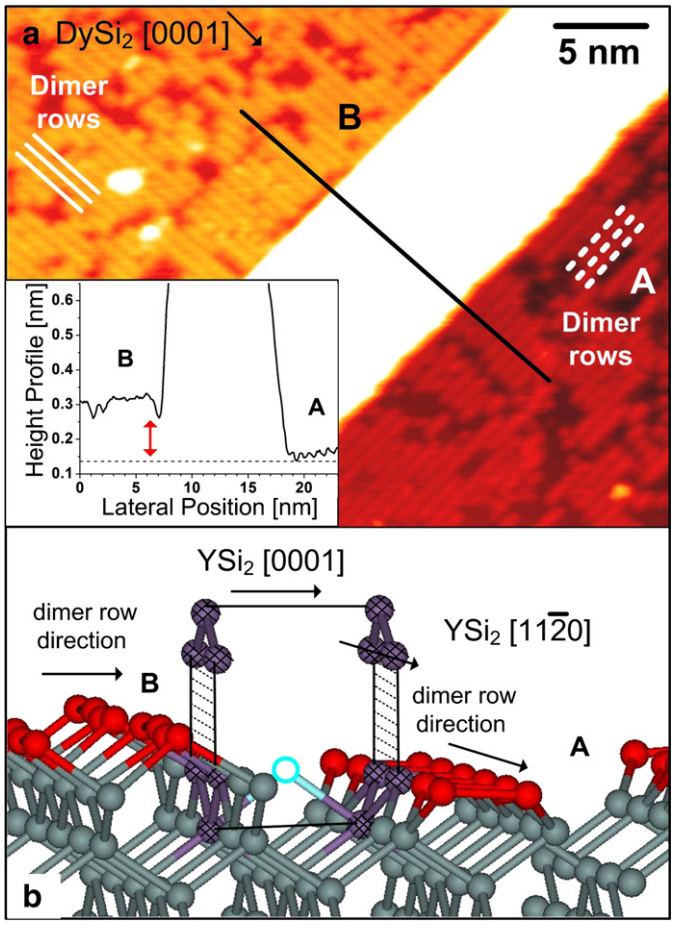

Fig. 2. (a) $DySi_{2-x}$ nanowire (running diagonally from the lower left to the upper right portion of the image) on flat Si(001) acquired with $V_{bias} = -2.0$ V and 200 pA feedback current. The dimer row direction on A-type terraces is highlighted by white dashed lines and dimer row direction on B-type terraces is highlighted by solid white lines. The inset in the left lower corner is a line profile along the black line in (a). (b) A schematic of a YSi_2 unit cell on Si(001) shows the atomic configuration of the surface and interface that is consistent with the data in (a), purple cross hatched spheres represent Si atoms in the YSi_2 unit cell, cyan open sphere represents Y, red spheres represent Si surface dimers, and gray solid spheres represent bulk Si.

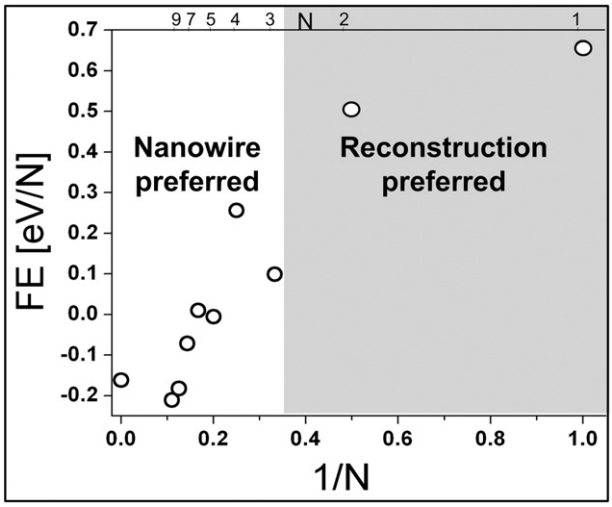

Fig. 3. Graph of formation energy versus inverse nanowire width for single disilicide layer nanowires (width $= N * a_{Si}$).

5, 6, and 7, respectively. Thus, FE calculations show a preference for nanowires having width of an odd multiple of a_{Si} for $N = 3$ through 7, as has been reported experimentally for YSi_2 nanowires on Si(001) [2,3]. It must be noted that the differences in FE given in the graph of Fig. 3 are normalized for the number of YSi_2 cells, thus when the total energy difference (FE times the number of cells in the system) is compared, the differences are significant. The point at $1/N = 0$ represents the formation energy of 1 full ML of YSi_2 calculated on a 1×10 substrate slab. The shallow FE energy curve is not surprising due to the meta-stability of these types of nanowires observed in experiments. At annealing temperatures of 750 °C and above, a phase transition to larger islands with the tetragonal crystal structure occurs [42–44]. Although adatom induced reconstructions have been reported to coexist with disilicide nanowires on Si(001), comparing STM images of $DySi_{2-x}$/Si(001) annealed at 600 °C with those annealed at 680 °C shows that the substrate has a higher coverage of Si dimer rows at the higher annealing temperature. This indicates that adatom incorporation in $DySi_{2-x}$ may be energetically preferred but limited by kinetic factors [20].

In order to understand the dependence of FE on nanowire width, the relaxed structures of YSi_2 wires having a width of 1 to 5 a_{Si} were calculated and are shown in Fig. 4(a)–(e). It is observed that Y atoms located in a trough between Si dimer rows, labeled Y_t, shift upward in relation to Y atoms located under a Si dimer pair, labeled Y_d. Strain within the nanowire, as a result of the 7.9% lattice mismatch [33] along the nanowire width, may be reduced by this alternating Y_t–Y_d buckling behavior [45]. The Si–Si distance under Y_t (~0.35 nm) is less than bulk ($a_{Si} = 0.384$ nm) and the Si–Si distance under Y_d (~0.48 nm) is slightly greater. This variation is expected to provide some relaxation along the disilicide/silicon interface as a transition from the bulk silicon structure to the AlB_2 structure. Y_t atoms for $N = 4$ do not exhibit the same alternating Y_t–Y_d buckling that occurs in $N = 3$ and 5 nanowires, that may provide strain relaxation. From examination of the relaxed structures, all of the Si surface atoms form (2×1) dimers on top of nanowires for $N = 1$, 3 and 5, as shown in Fig. 4(a), (c) and (e), respectively. In contrast, for the case of $N = 2$ and 4, not all Si nanowire surface atoms form (2×1) dimers. Apparently, dimer formation on top of nanowires is important for the reduction in FE by reducing dangling bonds on the surface. Similar DFT studies have been performed for freestanding YSi_2 nanowires [46], which show Si dimer reconstruction for the nanowire surface; however, the alternating Y_t–Y_d buckling observed in Fig. 4 does not occur. Strain relaxation of the misfit at the nanowire–substrate interface via buckling would not be necessary on a freestanding structure.

An STM simulation of the relaxed structure of a 3 a_{Si} nanowire from Fig. 4(c) with a sample bias of −1.5 V is shown in Fig. 5(a) and has surface features consistent with dimer formation on nanowire surfaces. Filled states experimental STM data shown in Fig. 5(b) for a 1 nm wide $DySi_{2-x}$ nanowire (labeled I) shows dimer row reconstruction on the nanowire surface, as observed in other work as well [2,47]. White circles have been added in order to illustrate the positions of individual Si surface atoms. As RE coverage increases, $RESi_{2-x}$ nanowires may increase in width or height. In order to explore stable morphologies at higher coverage, FE for 3 a_{Si}, 5 a_{Si} and 7 a_{Si} wide YSi_2 nanowires having a height of two disilicide layers were compared to those having a height of one disilicide layer. Nanowires having two YSi_2 layers were found to be 100–200 meV lower than single layer YSi_2 counterparts in agreement with experimental observations [27,48]. STM data of a $DySi_{2-x}$ nanowire shown in Fig. 5(c) verifies multilayer disilicide growth. The accompanying line profile (white line) shows feature heights of approximately 0.4 nm high for features on $DySi_{2-x}$ nanowire surfaces. This height is consistent with a second layer on the nanowire surface; one layer of the hexagonal cell of the $DySi_{2-x}$ is reported to be 0.35 nm high

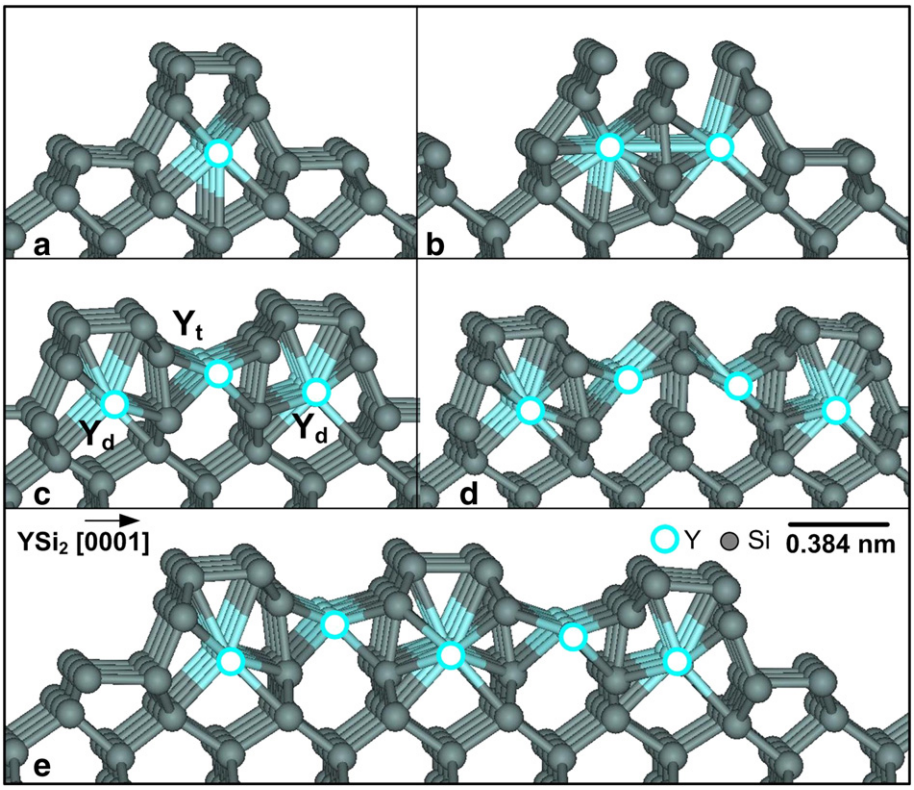

Fig. 4. YSi_2 nanowires having a width of (a) 1 a_{Si}, (b) 2 a_{Si}, (c) 3 a_{Si}, (d) 4 a_{Si} and (e) 5 a_{Si} are shown, $a_{Si} = 0.384$ nm. Y atoms are represented by cyan open spheres and gray spheres represent Si atoms. Y_t refers to Y atoms located in the trough between Si dimer rows and Y_d refers to Y atoms located under Si dimer pairs.

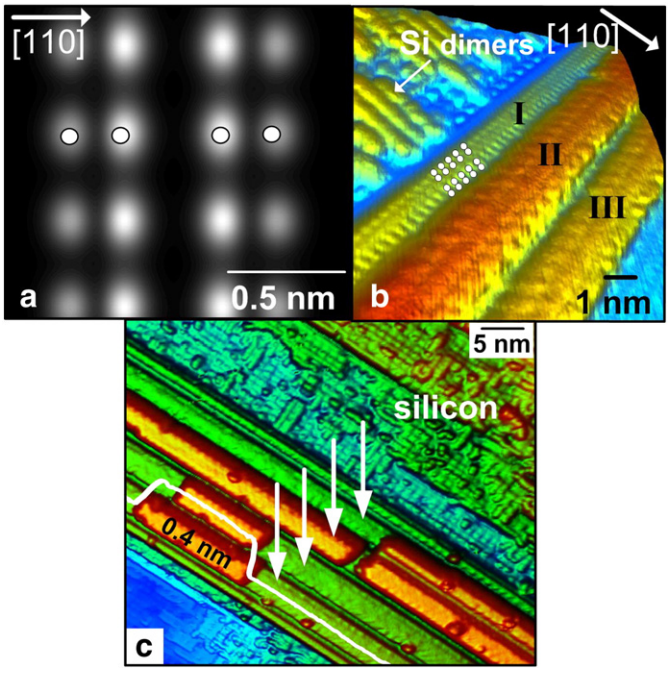

Fig. 5. (Cold to warm colors represent increasing feature heights) (a) Simulated STM image with $V_{bias} = -1.5$ V for a single YSi_2 nanowire with width = 3 a_{Si} and a single layer in height. (b) STM image of $DySi_{2-x}$ nanowires on flat Si(001), a nanowire with width = 3 a_{Si} and a single layer in height labeled I next to wider multilayer nanowires, labeled II and III, acquired with $V_{bias} = -1.85$ V and 100 pA feedback current. White open circles on nanowire I highlight Si atom positions on the nanowire surface that have the same periodicity as that of the simulation in (a). (c) STM image of $DySi_{2-x}$ nanowires (highlighted with white arrows) on miscut Si(001) acquired with $V_{bias} = -1.67$ V and 101 pA feedback current. A height profile (white line) is included on one of the wires to highlight multilayer growth on $DySi_{2-x}$ nanowires; the top layer is 0.4 nm above the initial nanowire layer.

[48,49]. Nanowires having width greater than 1 nm and multilayer height typically do not show dimer row reconstruction, as seen in Fig. 5(b) and (c), respectively. A variety of other nanowire surface reconstructions have been observed, such as $p(1\times1)$ and $c(2\times2)$, for $DySi_{2-x}$ [10,48] and $ErSi_{2-x}$ [50] nanowires. These may be due to Si vacancies, which are thought to reduce the strain caused by lattice mismatch [46]. Incorporation of vacancies into the atomic models is left for future work.

4. Conclusions

Synergistic *ab initio* calculations of Y/Si(001) and STM measurements of Er/Si(001) and Dy/Si(001) were performed for the orientation dependence of adatom induced reconstructions and disilicide nanowires on Si(001). We provide the first calculations that relate the atomic configurations in the wetting layer with the nanowire–substrate interface. The orientation of disilicide nanowires on Si(001) was explained as a result of a preference for adatoms to form atomic chains perpendicular to Si dimer rows on the clean Si (001) surface; these atomic chains are precursors to nanowires. Subsequent disilicide formation occurs as Si diffuses and reorganizes, therefore revealing dimer rows parallel to nanowire length on the plane of the nanowire–substrate interface. This is consistent with the wetting layer geometry where a coherent hexagonal disilicide nanowire–substrate interface must be formed with [1120] parallel to Si dimer row direction. Formation energy calculations reveal a preference for nanowires having widths = $N_{odd}a_{Si}$, governed by free energy reductions associated with Si dimer formation on nanowire surfaces and local relaxation of rare earth atom bonds in the interior of a nanowire. The calculated YSi_2 nanowire width predictions are in good accordance with STM images of $DySi_{2-x}$ nanowires that are one unit cell in the height direction. FE energy calculations show that as

Y coverage increases, full monolayer disilicide formation on Si(001) is not energetically favorable compared to second layer growth on YSi_2 nanowire surfaces, thus providing an explanation for multiple layer disilicide growth seen in experimental STM data of $DySi_{2-x}$ nanowires. The combination of theory and experiment has allowed a general comprehension of thermodynamic variables and morphology of nanostructures that cannot be understood through STM alone. This study provides information regarding atomic arrangement of adatoms and equilibrium nanowire structures that is essential for the utilization of this material system in future device applications.

Acknowledgments

Acknowledgment is made to the National Science Foundation CBET-0731349. Calculations were performed on NERSC supercomputers. AS and RR acknowledge T. Ayvazian for help with data analysis and Dr. Juexian Cao for help with STM simulations. AS acknowledges the UCI Graduate Dean's Dissertation Fellowship.

References

[1] J.W.G. Wildoer, L.C. Venema, A.G. Rinzler, R.E. Smalley, C. Dekker, Nature 391 (1998) 59.
[2] C. Zeng, P.R.C. Kent, T. Kim, A. Li, H.H. Weitering, Nat. Mater. 7 (2008) 539.
[3] V. Iancu, P.R.C. Kent, C.G. Zeng, H.H. Weitering, Appl. Phys. Lett. 95 (2009) 123107.
[4] C. Preinesberger, S. Vandre, T. Kalka, M. Dahne-Prietsch, J. Phys. D Appl. Phys. 31 (1998) L43.
[5] B.Z. Liu, J. Nogami, Nanotechnology 14 (2003) 873.
[6] R. Ragan, Y. Chen, D.A.A. Ohlberg, G. Medeiros-Ribeiro, R.S. Williams, J. Cryst. Growth 251 (2003) 657.
[7] Y. Chen, D.A.A. Ohlberg, R.S. Williams, J. Appl. Phys. 91 (2002) 3213.
[8] R.D. Thompson, B.Y. Tsaur, K.N. Tu, Appl. Phys. Lett. 38 (1981) 535.
[9] C. Preinesberger, G. Pruskil, S.K. Becker, M. Dahne, D.V. Vyalikh, S.L. Molodtsov, C. Laubschat, F. Schiller, Appl. Phys. Lett. (2005) 87.
[10] J. Nogami, B.Z. Liu, M.V. Katkov, C. Ohbuchi, N.O. Birge, Phys. Rev. B 63 (2001) (art. no.).
[11] H.W. Yeom, Y.K. Kim, E.Y. Lee, K.D. Ryang, P.G. Kang, Phys. Rev. Lett. (2005) 95.
[12] K.N. Tu, R.D. Thompson, B.Y. Tsaur, Appl. Phys. Lett. 38 (1981) 626.
[13] R. Ragan, et al., Proc. SPIE 5593 (2004) 167.
[14] J.P. You, J.H. Choi, S. Kim, X.M. Li, R.S. Williams, R. Ragan, Nano. Lett. 6 (2006) 1858.
[15] M. Valden, X. Lai, D.W. Goodman, Science 281 (1998) 1647.
[16] J. Grunes, J. Zhu, M.C. Yang, G.A. Somorjai, Catal. Lett. 86 (2003) 157.
[17] Y. Chen, D.A.A. Ohlberg, G. Medeiros-Ribeiro, Y.A. Chang, R.S. Williams, Appl. Phys. Lett. 76 (2000) 4004.
[18] G.F. Ye, J. Nogami, M.A. Crimp, Thin Solid Films 497 (2006) 48.
[19] A. Shinde, J. Cao, R. Wu, R. Ragan, Isr. J. Chem. 48 (2008).
[20] A. Shinde, J. Cao, S. Lee, R. Wu, R. Ragan, Chem. Phys. Lett. 466 (2008) 159.
[21] A. Shinde, J. Cao, W. Ouyang, R. Wu, R. Ragan, Phys. Lett. A 373 (2009) 3459.
[22] C. Ohbuchi, J. Nogami, Surf. Sci. 579 (2005) 157.
[23] J.S. Yang, Q. Cai, X.D. Wang, R. Koch, Surf. Sci. 526 (2003) 291.
[24] B.C. Harrison, P. Ryan, J.J. Boland, Surf. Sci. 582 (2005) 79.
[25] B.Z. Liu, J. Nogami, Surf. Sci. 488 (2001) 399.
[26] C. Ohbuchi, J. Nogami, Phys. Rev. B 66 (2002).
[27] A. Pratt, C. Woffinden, C. Bonet, S. Tear, Phys. Rev. B 78 (2008).
[28] B.Z. Liu, J. Nogami, Surf. Sci. 540 (2003) 136.
[29] G. Kresse, J. Furthmuller, Phys. Rev. B 54 (1996) 11169.
[30] L. Magaud, J.Y. Veuillen, D. Lollman, T.A.N. Tan, D.A. Papaconstantopoulos, M.J. Mehl, Phys. Rev. B 46 (1992) 1299.
[31] C. Rogero, C. Koitzsch, M.E. Gonzalez, P. Aebi, J. Cerda, J.A. Martin-Gago, Phys. Rev. B 69 (2004).
[32] C. Rogero, C. Polop, L. Magaud, J.L. Sacedon, P.L. de Andres, J.A. Martin-Gago, Phys. Rev. B 66 (2002).
[33] J.H.G. Owen, K. Miki, D.R. Bowler, J. Mater. Sci. 41 (2006) 4568.
[34] G. Kresse, D. Joubert, Phys. Rev. B 59 (1999) 1758.
[35] L. Magaud, A. Pasturel, G. Kresse, J. Hafner, Phys. Rev. B 55 (1997) 13479.
[36] D.J. Chadi, Phys. Rev. Lett. 59 (1987) 1691.
[37] W. Zhou, Y. Zhu, T. Ji, X.Y. Hou, Q. Cai, Nanotechnology 17 (2006) 852.
[38] G.F. Ye, M.A. Crimp, J. Nogami, Phys. Rev. B 74 (2006).
[39] M. Kuzmin, M.P.J. Punkkinen, P. Laukkanen, R.E. Perala, M. Ahola-Tuomi, T. Balasubramanian, I.J. Vayrynen, Phys. Rev. B 78 (2008).
[40] B.Z. Liu, J. Nogami, J. Appl. Phys. 93 (2003) 593.
[41] Y. Chen, D.A.A. Ohlberg, R.S. Williams, Mater. Sci. Eng. B-Solid 87 (2001) 222.
[42] Y. Zhu, W. Zhou, S.H. Wang, T. Ji, X.Y. Hou, Q. Cai, J. Appl. Phys. 100 (2006).
[43] A. Travlos, N. Salamouras, E. Flouda, Appl. Surf. Sci. 120 (1997) 355.
[44] S. Lee, A. Shinde, R. Ragan, Nanotechnology 20 (2009).
[45] Y. Chen, J. Washburn, Phys. Rev. Lett. 77 (1996) 4046.
[46] N.G. Szwacki, B.I. Yakobson, Phys. Rev. B 75 (2007).
[47] C. Preinesberger, S.K. Becker, S. Vandre, T. Kalka, M. Dahne, J. Appl. Phys. 91 (2002) 1695.
[48] B.Z. Liu, J. Nogami, J. Appl. Phys. 93 (2003) 593.
[49] Z.A. He, D.J. Smith, P.A. Bennett, Phys. Rev. B 70 (2004).
[50] J.S. Yang, Q. Cai, X.D. Wang, R. Koch, Surf. Interface Anal. 36 (2004) 104.